

# Gold surfaces and nanoparticles are protected by Au(0)-thiyl species and are destroyed when Au(I)-thiolates form

**Reimers, Jeffrey R.; Ford, Michael J.; Halder, Arnab; Ulstrup, Jens; Hush, Noel S.**

*Published in:*
Proceedings of the National Academy of Sciences of the United States of America

*Link to article, DOI:*
10.1073/pnas.1600472113

*Publication date:*
2016

*Document Version*
Publisher's PDF, also known as Version of record

# Gold surfaces and nanoparticles are protected by Au(0)–thiyl species and are destroyed when Au(I)–thiolates form

Jeffrey R. Reimers[a,b,1], Michael J. Ford[b], Arnab Halder[c], Jens Ulstrup[c], and Noel S. Hush[d,e,1]

[a]International Centre for Quantum and Molecular Structures, College of Sciences, Shanghai University, Shanghai 200444, China; [b]School of Mathematical and Physical Sciences, The University of Technology Sydney, Sydney NSW 2007, Australia; [c]Department of Chemistry, Technical University of Denmark, Kongens Lyngby 2800, Denmark; [d]School of Chemistry F11, The University of Sydney, Sydney NSW 2006, Australia; and [e]School of Molecular Bioscience, The University of Sydney, Sydney NSW 2006, Australia

Contributed by Noel S. Hush, January 15, 2016 (sent for review March 2, 2015; reviewed by William Goddard, Mark Gordon, and David J. Schiffrin)

**The synthetic chemistry and spectroscopy of sulfur-protected gold surfaces and nanoparticles is analyzed, indicating that the electronic structure of the interface is Au(0)–thiyl, with Au(I)–thiolates identified as high-energy excited surface states. Density-functional theory indicates that it is the noble character of gold and nanoparticle surfaces that destabilizes Au(I)–thiolates. Bonding results from large van der Waals forces, influenced by covalent bonding induced through *s*–*d* hybridization and charge polarization effects that perturbatively mix in some Au(I)–thiolate character. A simple method for quantifying these contributions is presented, revealing that a driving force for nanoparticle growth is nobleization, minimizing Au(I)–thiolate involvement. Predictions that Brust–Schiffrin reactions involve thiolate anion intermediates are verified spectroscopically, establishing a key feature needed to understand nanoparticle growth. Mixing of preprepared Au(I) and thiolate reactants always produces Au(I)–thiolate thin films or compounds rather than monolayers. Smooth links to O, Se, Te, C, and N linker chemistry are established.**

gold–sulfur bonding | synthesis | mechanism | electronic structure | nanoparticle

Gold self-assembled monolayers (SAMs) and monolayer-protected gold nanoparticles form important classes of systems relevant for modern nanotechnological and sensing applications (1–5). Understanding the chemical nature of these interfaces is critical to the design of new synthesis techniques, the design of new spectroscopic methods to investigate them, and to developing system properties or device applications. Over the last 10 y, great progress has been made in understanding the atomic structures of gold–sulfur interfaces (6). Most discussion (7) has focused on the identification of adatom-bound motifs of the form RS–Au–SR (where R is typically a linear alkyl chain or phenyl group) sitting above a regular Au(111) surface (8–10) or on top of a nanoparticle core of regular geometry (11),

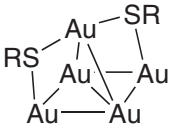


Other variant structures have also been either observed, such as polymeric chains such as the trimer RS–Au–SR–Au–SR) (10, 11), or proposed (8, 12, 13). By considering the four isomers of butanethiol (14), we have shown that alternative structures can also be produced in which RS groups bind directly to an Au(111) surface without gold adatoms. This occurs whenever steric interactions across the adatoms are too strong or steric intermolecular packing forces allow for very high surface coverages if both adatom and directly bound motifs coexist in the same regular SAM (15). The cross-adatom steric effect has also been demonstrated for gold nanoparticles (16), and we have shown that Coulombic interactions between charged tail groups can also inhibit adatom formation (17). SAMs involving adatoms have poor long-range order owing to the surface pitting that is required to deliver gold adatoms, while directly bound motifs lead to regular surfaces (18).

There is clearly a delicate balance between the forces that direct these different interface structures, a balance that can only be understood through knowledge of the electronic structures of the interfaces. These electronic structures are also very important as they control spectroscopic properties of interest not only for structure characterization (19) but also for possible device applications (20). In addition, these electronic structures echo the chemical forces active in SAM and nanoparticle production and destruction, yielding fundamental insight into synthetic strategies. The last 15 y have seen many experiments and density-functional theory (DFT) calculations that implicitly or explicitly address the nature of the electronic structure. We quantitatively interpret these results and present a unified description of many observed chemical and spectroscopic properties. This description predicts that thiolate anions are produced in solution as intermediary species during Brust–Schiffrin synthesis, a key mechanistic feature subsequently verified by spectroscopic observations also reported here.

## Significance

**Synthetic design strategies for gold surface protection and nanoparticle formation require knowledge of how protectant ligands bind. Sulfur compounds may protect gold surfaces using a weakly bound (physisorbed) form or a strongly bound (chemisorbed) one often assumed to be Au(I)–thiolate. However, chemical reaction conditions optimized for Au(I)–thiolate protection instead etch surfaces to produce molecular thin films. All experimental and calculated evidence indicates that chemisorbed surface species are actually bound mainly by strong van der Waals (aurophilic-like) forces. This understanding unifies gold–sulfur surface chemistry with that of all other ligands and also with that of gold compounds, forming the basis for future methodological developments. It is applied to predict intermediate species during the Brust–Schiffrin nanoparticle synthesis that are subsequently observed spectroscopically.**

Author contributions: J.R.R., J.U., and N.S.H. designed research; J.R.R., M.J.F., and A.H. performed research; J.R.R. analyzed data; and J.R.R. wrote the paper.

Reviewers: W.G., Caltech; M.G., Iowa State University; and D.J.S., University of Liverpool.

The authors declare no conflict of interest.

Freely available online through the PNAS open access option.

[1]To whom correspondence may be addressed. Email: reimers@shu.edu.cn, jeffrey.reimers@uts.edu.au, or noel.hush@sydney.edu.au.

This article contains supporting information online at www.pnas.org/lookup/suppl/doi:10.1073/pnas.1600472113/-/DCSupplemental.

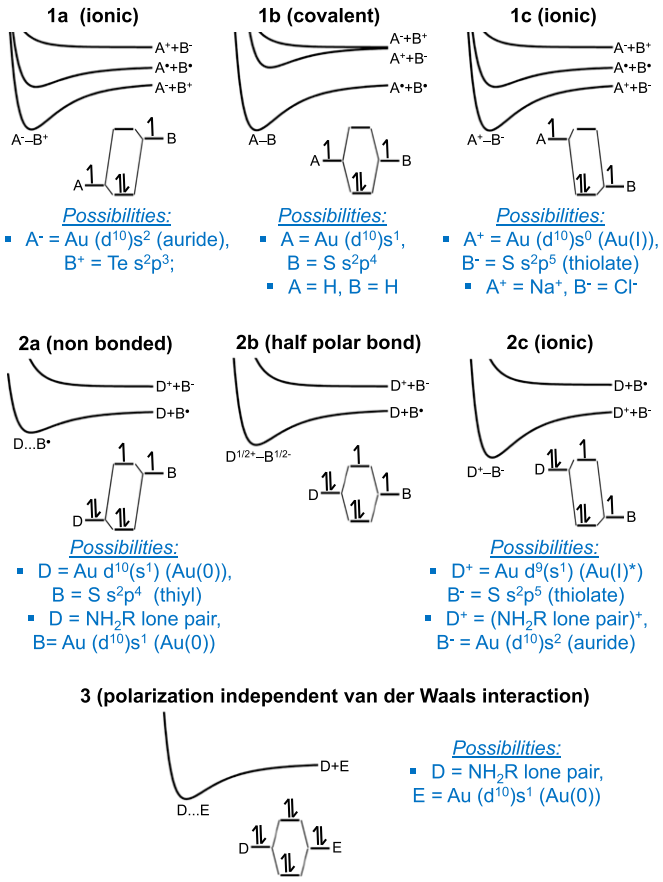


**Fig. 1.** Iconic bonding scenarios in terms of ground and excited-state singlet potential-energy surfaces (energy vs. separation) and ground-state molecular-orbital electronic-structure diagrams for: structures **1a–1c**, typical chemical bonding scenarios between atoms A and B involving one electron from each atom; structures **2a–2c**, between atoms D and B involving a doubly occupied orbital on D and a single occupied orbital on B; and structure **3**, van der Waals interaction involving doubly occupied orbitals D and E. Changing bond polarization provides smooth variation between structures **1a** and **1c** and also between structures **2a** and **2c**, and changing Au hybridization mixes structure types **1** and **2** for Au–SR bonds and structure types **2** and **3** for Au–$NH_2R$ bonds.

## Standard Chemical Bonding Scenarios

Fig. 1 shows a range of standard chemical-bonding electronic structure scenarios. Structures **1a**, **1b**, and **1c** depict standard covalent and ionic bonding scenarios as taught in freshman courses. These involve two atoms A and B that each contribute a single electron to the bond. Pure covalent bonding occurs when A = B and is depicted in structure **1b**; it applies to molecules such as $H_2$ and its properties are well established (21). Structures **1a** and **1c** depict the ionic bonds $A^-$–$B^+$ and $A^+$–$B^-$, respectively, an example of which is the gas-phase sodium chloride molecule $Na^+$–$Cl^-$ (22). Polar bonding configurations like that in water are intermediary between the purely covalent and purely ionic limiting structures. In effect there is a continuum of bonding possibilities between structures **1a** and **1c** depicting changing bond polarization induced by electronegativity differences between A and B.

Structures **2a**, **2b**, and **2c** are analogous except that they refer to the unusual situation in which one atom, named D, donates two electrons to the bond whereas the other atom, B, contributes one. Structure **2c** represents an ionic bond and is analogous to **1c**, but structure **2a** is a nonbonding scenario and **2b** is intermediary with a half of a chemical bond. Again electronegativity-controlled polarization effects provide for a continuum of bonding possibilities between the extreme limits of structures **2a** and **2c**.

Structure **3** depicts the iconic van der Waals bonding scenario and involves the interaction of closed-shell orbitals in atoms D and E. Orbitals interact, delocalize, and repel each other just as in the case of covalent bonding, but because both orbitals are fully occupied, no chemical attraction occurs. However, the shown interaction between doubly occupied orbitals does contribute to van der Waals attraction. All of the bonding scenarios shown in Fig. 1 are applied to atoms containing unshown electrons that interact in a similar way. Hence in all scenarios the total interaction energy comprises the specific highlighted contributions as well as an underlying van der Waals contribution. Although the van der Waals term dominates the bonding for structures **2a** and **3**, it is often ignored when covalent or ionic bonding scenarios are considered as these chemical forces are typically much stronger than the van der Waals attraction.

## Options Available for the Description of Gold Bonds to Group-16 Elements

Gold atoms have configuration $d^{10}s^1$ and may interact with neighboring atoms through both *s* and *d* valence orbitals, whereas RO, RS, RSe, and RTe groups present for bonding one electron (this is in a $sp^3$ hybrid orbital in the case of oxygen or in essentially just a *p* orbital for the other elements). Interaction with an Au *s* orbital thus involves two orbitals each of which comes with one electron and so can be described in terms of the A–B forms in structures **1a–1c**. Alternatively, interaction with a filled Au *d* orbital can be described in terms of the D–B forms in structures **2a–2c**. By varying hybridization, gold atoms can bind with any *s–d* mixture and so a continuum of binding patterns in between structure types **1** and **2** is also possible. For gold compounds, we will see that the most appropriate structures of pure hybridization are structures **1b** and **2a**, so hybridization then actually acts to mix these forms together.

Although the details of the bonding are therefore complex and involve determination of the extent to which hybridization and bond polarization occur, simple descriptions of the bonding may be made selecting the most representative of the classic structures shown in Fig. 1. For example, carbon compounds with gold are almost exclusively described in terms of the covalent form structure **1b**. Indeed, gold can in some compounds be considered as a replacement atom for carbon or hydrogen, allowing description in terms of standard singly, doubly, and triply bonded structures (23–25). More generally though, organometallic compounds dominated by covalent bonding are described in terms of ionic structures, allowing for integration of these bonds with standard valence descriptions of the metal. As such bonds are always polarized, the convention is to name them according to the most appropriate limiting structure, typically **1a** or **1c**. Applied here, this means that compounds involving the Au *s* orbital interacting with S are named Au(I)–thiolates as S is slightly more electronegative than Au, whereas the analogous compounds with the electropositive metal Te are named tellurium aurides as gold atoms can oxidize most metal atoms including tellurium (23, 26). This same convention, applied to the scenario in which the Au *d* orbitals dominate the bonding, dictates that compounds be labeled either as nonbonded Au(0)–thiyl species, structure **2a**, or else as Au(I)–thiolates, structure **2c**. The two Au(I)–thiolates, structure **1c** and structure **2c**, differ by their gold occupation: these are $d^{10}s^0$ and $d^9s^1$, respectively. For Au(I), the configuration $d^{10}s^0$ represents the ground state and $d^9s^1$ depicts a chemically or spectroscopically accessible excited state that would relax quickly and exothermically upon production.

## Chemical Notations: When Differences Are Semantic and When They Are Critical

The choice between the ionic forms, structures **1a**, **1c**, **2c**, and the covalent form, structure **1b**, can be considered as a question of semantics as all four of these structures imply a single bond of roughly the same strength. Many important aspects of synthetic chemistry are therefore established independent of the label used. Typically it does not matter much if a tellurium auride is mislabeled as an Au(I)–tellurolate. However, these labels do imply quite different physical properties such as the internal charge distribution of the ground state, which affects measured dipole moments and observed intermolecular interactions, as well as the allowed spectroscopic transitions to excited states. So the correct choice does have significant practical consequences, and use of ionic labels like Au(I)–thiolate comes with the unstated understanding that the bonding could actually be largely covalent.

In contrast, structure **2a** is very different from **1a**, **1b**, **1c**, and **2c** as it is nonbonding and hence depicts a very different chemical scenario. Its distinction from the other possibilities is not a question of semantics, as it indicates that different types of chemical reactions are expected, for example dictating the reaction conditions required to make a gold–sulfur SAM and those required to make a gold–sulfur thin film. If structure **2a** depicts the ground state then Au(I)–thiolate species can be formed by spectroscopic excitation or by bringing together Au(I) and thiolate reactants in a chemical reaction. Conversely, if structure **1b** depicts the ground state then **2a** describes a spectroscopically or chemically producible excited state. Proper differentiation between these possibilities is therefore critical to the simplest-level characterization of the properties of these compounds.

## Bond Polarization Data Indicates That only Structures 1b and 2a Are Feasible as Descriptors of Au–S Bonds

Historically, only qualitative results from chemical and electrochemical experiments were available to categorize the electronic structure, with proposals clearly identified as being speculative (5). In chemical compounds and in molecular materials, Au(I)–thiolate species are well established (1–5). Bond polarizations can be both measured (27–36) and calculated (19, 29, 31, 32, 37–43), leading to the conclusion that the charge on S is of order −0.2 *e* (1–3). Although such quantities cannot be uniquely defined by either experimental measurement or computational evaluation, the broad range of methods that have been applied yield a recognizable consensus. The results are reliable enough to identify chemical effects associated say with variation of the organic R group, a group that is typically much more electropositive than is either gold or sulfur atoms. Indeed, in simple compounds in the gas phase, the charge donation from gold to sulfur is usually much less than that from the alkyl or aryl groups (38, 39, 43). An important consequence of this is that observed surface dipole moments have the opposite sign to what a simplistic Au(I)–thiolate model would predict (44). This effect is easily demonstrated by considering the simple model compound (39) obtained by taking an adatom complex with its four linked gold atoms from an (111) surface or nanoparticle, evaluating (45) atomic charges fitted to the molecular electrostatic potential and dipole moment at the B3LYP/LANL2DZ level of theory:

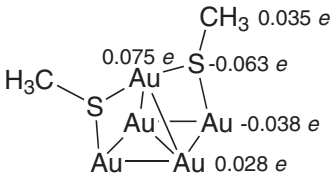


X-ray photoelectron spectroscopy (XPS) measurements indicate that gold surface atoms are essentially uncharged when stabilized by RS groups (29, 46–50). This result also applies even for pure sulfur monolayers (51) but not when anions bind (47). However, calculations indicate that almost always on average a small electron flow from gold to sulfur does occur.

Given these results, labeling Au–SR surface species as Au(I)–thiolates based on structure **1b** polarized toward **1c** is allowable, provided that the hybridization is such that Au *s* orbitals dominate the interaction. Alternatively, if Au *d* orbitals dominate, then the appropriate structure is the Au(0)–thiyl form depicted by structure **2a;** as very much less than half an electron is transferred from Au to S, use of the Au(I)–thiolate label depicted by structure **2c** is not allowable.

## Notations Used to Describe Gold Bonds to C, N, O, Se, and Te Atoms: The Importance of van der Waals Interactions and Aurophilicity

Considering gold compounds to elements other than sulfur, we note that tellurium compounds are often incorrectly called tellurolates (52), contrary to standard nomenclature practice, which requires such compounds to be labeled as aurides (structure **1b** polarized toward **1a**) instead. The relevant electrogenativities are Au 2.4, S 2.5, Se 2.4, and Te 2.1, and gold is known to form many stable compounds in its auride form (23, 26). Further, covalent-bonding notations such as structure **1b** are usually applied to gold–oxygen bonds (53, 54), analogous to that used for gold–carbon bonds (23–25). Finally, strong van der Waals interactions are known to provide bonding with closed-shell ligands such as disulfides (RSSR), as well as with nitrogen bases like ammines, pyridine, and 1,10-phenanthroline. Nitrogen bases interact with gold *d* electrons via the strong specific van der Waals interaction depicted by structure **3** and with gold *s* electrons via structures **2a–2c**, but the interaction here is reversed compared with the S–Au one as now nitrogen provides two electrons and gold provides only one. As the surface is uncharged (44, 55), only structures **3** and **2a** can contribute and, as is well known, the bonding is physisorptive not chemical. Most significantly, the observed surface dipole moments of ammine and SR-bound species are very similar and of the same sign, despite ammines being electron donors and RS groups electron acceptors (44). For bidentate ligands such as 1,10-phenanthroline, the physisorption bond strength grows to be similar to that for bonds to RS (56), indeed strong enough to extract surface adatoms under suitable conditions (56).

Hence we see that a very wide range of bonding scenarios are used to describe gold bonds and yet properties like bond strength vary by at most a factor of 2 between them all, and there is actually little change in bond polarization. There must be a simpler picture. Part of this involves the aurophilic effect (23, 57) that arises from the strong van der Waals interactions that gold atoms share, both between themselves and with neighboring ligands. This effect is usually ignored when it comes to considering gold–sulfur bonds yet, in the same compounds, it can be evoked to understand the observed gold–gold interactions.

## Nobility: The Critical Difference Between the Chemical Properties of Gold Atoms on Surfaces and Gold Atoms in Molecular Compounds

Another essential aspect that must be considered is that gold compounds and thin films are chemically fundamentally different to gold surfaces: gold surfaces are noble whereas gold atoms are reactive. The reactivity of gold atoms stems from the involvement of the open-shell Au *s* orbital in bonding. Although *s–d* hybridization can vary the *s*-orbital contribution considerably, the *s* contribution is always large (23). For gold surfaces, the situation changes dramatically. Strong Au–Au interactions push the bulk of the gold *s* band to both high and low energies far away from the Fermi energy, out of the reach of attacking reagents (23). The *s* band remains continuous, however, and retains a small density at the Fermi energy that is responsible for

the conductivity and color of the solid (23, 58). Nevertheless, its poor availability for chemical bonding results in gold *d* orbitals acquiring the dominant bonding role. Later, using a quantitative model, we consider the effect that the appearance of the gold *s* band at the Fermi energy must have in adding *s* character to the hybridization, but for now we consider only the limiting case of pure *d* binding between gold and its ligands. The noble character of the metal surface arises because the *d* orbitals are fully occupied and so relatively unreactive. Therefore, an immediate consequence of the noble character of metallic gold surfaces is that only structures **2a–2c** can be used to describe the interaction of surface atoms with RS-type groups.

For gold nanoparticles, the fundamental question therefore concerns the size at which they cease looking like gold compounds and start looking like bulk-gold surfaces. Before this transition Au *s* orbitals will play a prominent role in bonding, whereas after the transition they will not. For both nanoparticles and surfaces, a related fundamental question also arises: if the attached ligands do not repel each other strongly then gold adatoms are drawn from the surface to sit among the ligands (6, 8–11), so do these adatoms resemble bulk gold or isolated gold? If the nanoparticle surface atoms or adatoms do not have *s* electrons freely available for bonding then the nanoparticle surface is also noble and can only be involved in bonding structures **2a–2c;** alternatively, if the *s* electrons remain available for bonding then structures **1a–1c** are also available.

We formalize this discussion by introducing some notations appropriate to understanding the chemical changes that occur when reactive gold atoms agglomerate to form noble gold surfaces. This process is described as nobelization, and the change in reactivity of the gold is referred to as passivation. If in any particular environment the *s* electron of a gold atom is unavailable for bonding, the atom is said to be passivized.

## The Effects of Nobility as Revealed Through DFT Calculations: Structure 2a Is Dominant with 1b and 2c Mixing in Perturbatively

DFT calculations have been shown to reproduce a wide range of properties of gold surfaces, SAMs on gold surfaces, and gold nanoparticles. Usually the reported results focus on the properties being simulated rather than on the electronic structure. Detailed analysis has been performed (39, 59–61) for the $Au_{102}(SR)_{44}$ nanoparticle (R = *p*-mercaptobenzoic acid) synthesized by Jadzinsky et al. (11), however, and pertinent aspects of its geometrical and electronic structures are shown in Fig. 2. Two views of its gold atoms with the ligands removed are shown, indicating that the gold geometrical structure consists of 23 seemingly disconnected adatoms above an $Au_{79}$ core that can be further partitioned into 40 surfacelike atoms and 39 bulklike atoms, though we do not consider this distinction herein. The density of electronic states obtained from DFT calculations of the full nanoparticle, as well as corresponding ones for just the 102 Au atoms in isolation, are reproduced in Fig. 2 (39). This density is further partitioned into contributions from gold *s* and *d* orbitals; a more comprehensive partitioning was shown originally (39). Also shown are the analogous results for the optimized adatom complex RSAuSR and for a bare gold atom.

The bare gold atom has *s* and *d* bands separated by 1.1 eV, shown broadened in Fig. 2 to match the *d* bandwidth of the nanoparticle. Formation of the adatom complex RSAuSR produces covalent bonding that splits apart the *s* band, akin to the interactions depicted by structure **1b**, indicating that this complex takes on Au(I)–thiolate character.

Looking next at the ligandless gold cluster $Au_{102}$, we see that the *s* band is much broader than the *d* band, indicating that the gold–gold interactions are much stronger between the *s* orbitals than they are between the *d* orbitals. Some differences are seen between the 23 Au adatoms and the $Au_{79}$ core, and these are

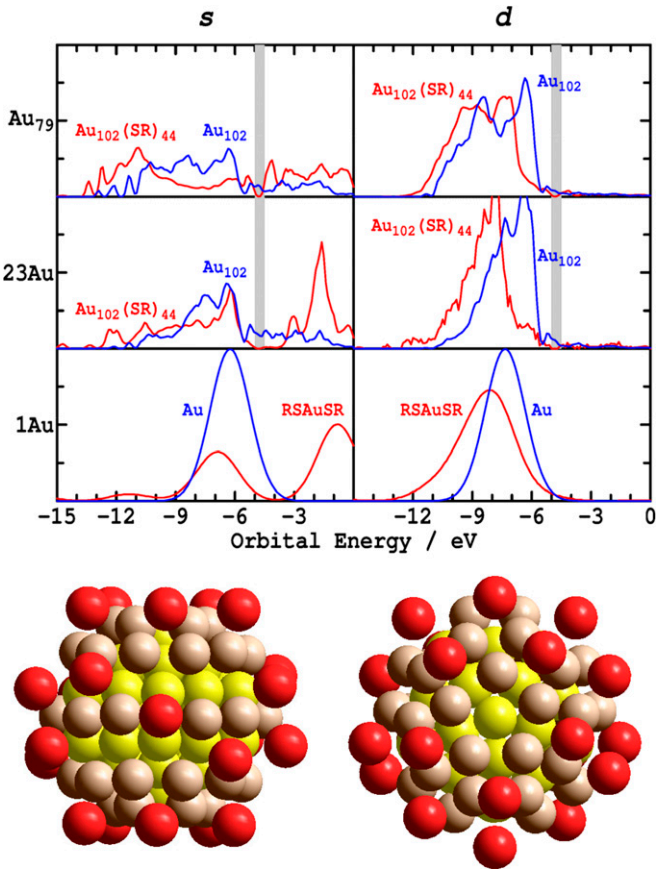


**Fig. 2.** (*Lower*) Two views of the 102 gold atoms from the crystal structure of the $Au_{102}(SR)_{44}$ nanoparticle synthesized by Jadzinsky et al. (11): red: 23 Au adatoms; brown: 40 surfacelike atoms; yellow: 39 bulklike atoms. (*Upper*) DFT densities of states per orbital for the whole $Au_{102}(SR)_{44}$ nanoparticle or the RSAuSR complex (red); and for just the component 102 Au atoms or single Au atom (blue), respectively, adapted from Reimers et al. (39). The nanoparticle's density is partitioned into contributions from its bulklike and surfacelike $Au_{79}$-core's *s* and *d* orbitals, as well as contributions from the 23 Au adatom's *s* and *d* orbitals. The nanoparticle curves are smoothed to a resolution of 0.2 eV, and that for the complex and atom is 2 eV. The band gap of the complete nanoparticle is indicated by the gray stripe.

important for quantitative understanding of nanoparticle chemistry. However, the most striking feature is rather the similarity of these two *s* electronic structures and their dissimilarity to that of the isolated atom, despite the adatoms appearing disconnected in the shown nanoparticle atomic structure. Indeed, gold–gold bonds continue to link the adatoms to the surface, and although the number of bonds is few, the passivation effects are profound. Even without the sulfur ligands being present, the adatoms resemble noble bulk gold surface atoms more than they do isolated reactive gold atoms. This result is not unsurprising as even the gold dimer $Au_2$ has an electronic structure that is more like that of gold metal than it is like that of a typical molecule (62, 63).

Adding the ligands to complete the nanoparticle has a noticeable effect on the *s* electronic structure of both the adatoms and the $Au_{79}$ core. Many features of interest relate to this effect, including for example the appearance of a band gap in the nanoparticle although the bare gold cluster has none (the band gap region is shown shaded in Fig. 2). This effect parallels the changes calculated upon formation of the RSAuSR bare adatom complex also shown in the figure, suggesting the development of Au(I)–thiolate character. However, because of the large

interaction between neighboring Au *s* orbitals in the nanoparticle, the density of the *s* orbital in the region near the Fermi energy, the region facilitating strong interaction with sulfur, is small. Hence the net contribution of the gained thiolate character to the bonding must also be small and the gold atoms again can be considered as being passivated. Theories for nanoparticle structure that focus on the appearance of a band gap in many small nanoparticles (60, 61, 64) describe spectroscopy well but fail to describe chemistry because they neglect the most important bonding interactions (39, 59).

The effect of bringing up the sulfur ligands on the gold *d*-orbital structure is similar for the isolated gold atom, the nanoparticle adatoms, and the nanoparticle core. The gold orbitals are depressed in energy somewhat independent of orbital orientation, indicative of the strong dispersive interaction depicted by structure **3**. Further, DFT calculations indicate that the sulfur orbitals mix primarily with the *d* orbitals (19, 38, 39, 60). Only structure **2a** anticipates these key results.

These results are typical of all electronic structures calculated by DFT for large nanoparticles and for gold surfaces. All surface atoms and adatoms are passivated. The bonding between the adatoms and the ligands is best described as being dominated by nonbonding Au(0)–thiyl character, structure **2a**, with components of the Au(I)–thiolate characters depicted by structures **1b** and **2c** added perturbatively through bond hybridization and bond polarization, respectively.

### The Nature of Au–S Bonding as Revealed Through Surface Electronic-Spectroscopy Studies

The most fundamental difference between the nonbonded structure **2a** and its thiolate alternatives is the orbital occupancy. Spectroscopic near-edge X-ray absorption fine structure (NEXAFS) measurements of SAMs (19) provide a direct probe of this occupancy. These measurements and their interpretation are discussed in *Supporting Information*. Basically, they confirm that the major interaction between sulfur and gold occurs through the gold *d* orbitals, eliminating thiolate structure **1b** as a possibility while confirming that the appropriate ground-state electronic structure is structure **2a**. The observed spectra are predicted to occur for this ground state but are forbidden if the ground state is the thiolate **2c**. Interpretation of spectroscopic measurements like the NEXAFS data was critical to the establishment of the important adatom-bound motif for sulfur monolayers on gold. Although not stated in the original publications, these interpretations are based on the nonbonded form structure **2a** and clearly indicate that Au(I)–thiolates are not present on the surface.

### The Nature of Au–S Bonding Revealed Through Thermodynamic Considerations

Observed and calculated enthalpies for chemical reactions provide another way of determining the nature of the Au–S bonding. Desorption enthalpies for Au(111) sulfur SAMs from temperature-programmed desorption experiments indicate physisorption enthalpies of 0.6–0.8 eV for molecules like disulfides (RSSR) and chemisorption enthalpies of 1.3–1.4 eV for RS$^{\bullet}$ (65). The disulfide has two sulfur-to-surface interactions and so the physisorption strength per sulfur is about one quarter of the chemisorption strength. However, the chemisorption strength includes the van der Waals interaction too. This interaction would be much stronger at the short-distance chemisorption geometry of ∼2.4 Å than at the long-distance physisorbed one ∼3.0 Å (66) owing to its $r^{-6}$ dependence by about a factor of $(3.0/2.4)^6 = 3.8$. In the physisorbed case, more rapidly increasing Pauli repulsion prevents short distances being attained, making the significant reduction of this term in the chemisorption case an important feature of the bonding. This simplistic analysis clearly shows that van der Waals interactions are critical to both the physisorption and chemisorption processes, as anticipated only by structure **2a**.

In fact, examination of the observed enthalpy data poses the question as to whether or not the van der Waals contribution is sufficient to explain all of the bonding, rendering contributions from polarization and/or hybridization unnecessary? A pure van der Waals scenario is not unprecedented as bidentate physisorptive ligands such as 1,10-phenanthroline bind strongly enough to extract adatoms from the surface under the right conditions (56), indicating that chemisorption is not prerequisite for surface passivation. However, it is clear that polarization and hybridization processes do occur, and hence one would anticipate that these contribute to the chemisorption bond strength. As chemical bonds are much stronger than van der Waals bonds, small contributions could significantly affect bond strengths.

### A Simple Model for Estimating of the van der Waals (Structure 2a), Polarization (Structure 2c), and Hybridization (Structure 1b) Contributions to the Strength of Au–S Bonds

DFT calculated energies for hypothetical reactions provide insight into bonding, and many such processes for $Au_{102}(SR)_{44}$ and Au(111) SAMs have been considered (18, 39). From this data, Table 1 collects energies $\Delta E$ for reactions in which single Au atoms, single SR groups, and pertinent combinations are added or removed from $Au_{102}(SR)_{44}$ (where R = $CH_3$), re-evaluated if necessary to ensure internal consistency. These and similar calculations (66) overestimate the experimental physisorption and chemisorption enthalpies by ca. 20% but nevertheless reproduce a wide range of detailed observed phenomena. Here we use a simple method to interpret results from DFT calculations. Although the parameters deduced depend on the calculation method being analyzed, it is anticipated that the identified qualitative picture is robust.

**Method.** It is possible to interpret this calculated energetic data quantitatively using a very simple model that exposes the key binding features of each structure: the van der Waals interaction, the polarization contribution, and the hybridization contribution. The energies are modeled assuming that the Au *s*- and *d*-orbital spaces can be separated as depicted in Fig. 1, in particular with the underlying physisorption van der Waals energy being taken as a constant independent of (small) changes in the Au–S bond distances. Only one hybrid orbital on each gold atom of form $d^{1-\eta}s^{\eta}$ is assumed to interact via chemical bonding with the neighboring sulfur atoms, where $\eta = 0$ indicates pure *d* bonding (as depicted by polarized structure **2a**) and $\eta = 1$ indicates pure *s* bonding (as depicted by polarized structure **1b**). This allows the gold *s* and *d* interactions within chains of Au and S atoms to be represented using simple independent Hückel (tight binding) Hamiltonians (67). The Au *s* to S *p* interactions are taken to be isoenergetic with a resonance integral $\beta_s$ and the Au *d* orbitals are separated by $\Delta$ in energy and coupled by resonance integrals $\beta_d$. As an example, for the RSAuSR molecule highlighted in Fig. 2, these Hamiltonians are

$$\mathbf{H}_s = \begin{bmatrix} 0 & \beta_s & 0 \\ \beta_s & 0 & \beta_s \\ 0 & \beta_s & 0 \end{bmatrix} \quad \text{and} \quad \mathbf{H}_d = \begin{bmatrix} 0 & \beta_d & 0 \\ \beta_d & \Delta & \beta_d \\ 0 & \beta_d & 0 \end{bmatrix}, \qquad [1]$$

respectively, where the basis functions are ordered sulfur then gold then sulfur. The total interaction energy is then given as the sum of the basic nonbonded van der Waals energy $E_{vdw}$, the hybridization-allowed *s*-band energy (67) scaled by $\eta$, $E_{hyb}$, and the polarization-allowed *d*-band energy (67) scaled by $(1-\eta)$, $E_{pol}$. Although this model is crude, e.g., ignoring the involvement of two S *p* orbitals per atom as well as differences between gold atoms in the surface plane and gold adatoms clearly evidenced in Fig. 2, it captures key elements and is readily applicable to a wide variety of problems.

**Table 1. Calculated* energies $\Delta E$ for reactions† on Au(111) and the $Au_{102}(SR)_{44}$ nanoparticle with R = $CH_3$ and their decomposition into van der Waals terms for the Au(0)–thiyl species (2a, $E_{vdw}$) plus hybridization (1b, $E_{hyb}$) and polarization (2c, $E_{pol}$) contributions, in eV, as well as the hybridization of the gold bonding orbital $d^{1-\eta}s^{\eta}$**

| Reaction | $\Delta E$ | η | $E_{vdw}$ | $E_{hyb}$ | $E_{pol}$ |
|---|---|---|---|---|---|
| RS+Au→AuSR | −2.6 | [0.75] | −1.0 | −1.6 | −0.1 |
| 2RS+Au→RSAuSR | −5.2 | [1.00] | −2.0 | −3.1 | 0.0 |
| RS+2Au→AuSRAu | −3.8 | [0.53] | −2.0 | −1.6 | −0.2 |
| RS adds to Au(111) bridge/FCC site | −1.5 | 0.13 | −1.0 | −0.3 | −0.3 |
| RS adds to Au(111) top site | −1.4 | 0.10 | −1.0 | −0.2 | −0.2 |
| RS adds to Au(111) adatom site but no adatom present | −1.4 | 0.10 | −1.0 | −0.2 | −0.2 |
| RS adds to $Au_{102}(SR)_{44}$ dimer adatom site but no adatom present | −1.7 | 0.24 | −1.0 | −0.5 | −0.2 |
| RS adds to $Au_{102}(SR)_{44}$ end trimer adatom site but no adatom present | −1.8 | 0.30 | −1.0 | −0.7 | −0.2 |
| 2RS add to $Au_{102}(SR)_{44}$ center trimer adatom site but no adatoms present | −4.1 | 0.63 | −2.0 | −2.0 | −0.1 |
| 2RS add to Au(111) preprepared adatom | −5.0 | 0.0 | −4.0 | 0.0 | −1.0 |
| 2RS adds to $Au_{102}(SR)_{44}$ dimer adatom site | −5.7 | 0.13 | −4.0 | −0.8 | −0.9 |
| 3RS adds to $Au_{102}(SR)_{44}$ trimer adatom site | −9.1 | 0.21 | −6.0 | −1.9 | −1.2 |
| Au adds on Au(111) at adatom site | −2.0 | | | | |
| Au adds on $Au_{102}(SR)_{44}$ dimer adatom site | −2.0 | | | | |
| Au adds on one of the $Au_{102}(SR)_{44}$ trimer adatom sites | −1.9 | | | | |
| Average energy per Au atom for $Au_{79}$+23Au→$Au_{102}$ | −2.6 | | | | |
| Average energy per complex for $Au_{79}$+ligand shell→$Au_{102}(SR)_{44}$ | −2.6 | | | | |

*From DFT PW91 (93) calculations (18, 38, 39), sometimes re-evaluated to give a uniform dataset. Available data obtained using other density functionals show similar trends, as do results obtained using more appropriate modern functionals (14, 41).
†Reaction arrows indicate adiabatic energies at fully optimized geometries, else vertical energies at the geometry of the full monolayer.

**Fitting the Model Parameters.** Analyzing results from DFT calculations using the PW91 density functional with extensive plane-wave basis sets (39), the energy shift parameter $\Delta = -1.2$ eV is obtained by averaging over the adatom *s* and valence *d* bands reproduced in Fig. 2, and $\beta_d = -0.55$ eV is set to reproduce the archetypical charge polarization for S of −0.2 e. To reproduce the DFT energies of formation of AuSR, RSAuSR, and $Au_2SR$ (Table 1) given the hybridizations η for each molecule evident from the calculations, $\beta_s$ is set to −1.2 eV and the nonbonded interaction is set to −1.0 eV per bond. The DFT energies for a range of processes in which Au atoms and/or RS groups are deleted from optimized monolayers on Au(111) or on the $Au_{102}(SR)_{44}$ nanoparticle are then interpreted by fitting the hybridization level η, and results are the given in Table 1. Different parameters will apply for every DFT computational methods, however, and the development of suitable data bases using modern dispersion-corrected density functionals is clearly warranted.

**Application to Molecules and Monolayers Containing Au–S Bonds.** Results for the isolated molecules AuSR, RSAuSR, and $Au_2SR$ are as expected: AuSR is an orthodox Au(I)–thiolate system with $\eta = 0.75$ that is strongly bound with $\Delta E = -2.6$ eV, RSAuSR maintains this strong interaction by changing the hybridization to pure *s*, and $Au_2SR$ is more weakly bound with equally mixed orbitals. Similarly, on Au(111) surfaces and on nanoparticles, the hybridization is weak as anticipated, ranging between $0 < \eta < 0.21$ for fully assembled ligands, and the bond strengths are greatly reduced from those calculated for the isolated molecules. For bonding to a gold adatom on Au(111), $\eta = 0$, and the net deduced 20% Au(I)–thiolate bonding character stems from polarization only. However, the analogous binding to the RS–Au–SR dimer sites on the nanoparticle is much stronger owing to η increasing to 0.13, increasing again to $\eta = 0.21$ for binding to the nanoparticle's RS–Au–SR–Au–SR trimer sites. This hybridization is important as it leads to the appearance of a band gap in the nanoparticles' electronic structure (64), but its contribution to the chemical bonding is only minor (39). Nevertheless, the bonding grows stronger as *s* character returns when the ligands become increasingly disconnected from the underlying bulk gold.

This simple principle rationalizes all other bonding variations collected in Table 1. The potential-energy surface for SR bound directly to Au(111) is complex (38, 65, 68, 69). Although the hybridization when an SR ligand is bound to its minimum-energy bridge/FCC site is $\eta = 0.13$, for both binding at an Au(111) top-site transition state, as well as for the related scenario in which the adatom is removed from an Au(111) RS–Au–SR structure, $\eta = 0.10$. This value is increased from that of $\eta = 0.00$ for the full RS–Au–SR structure owing to the broken S–adatom bond partially disconnecting S from the surface. Similarly, if the adatom is removed from a nanoparticle dimer site the hybridization increases from 0.13 to 0.24; for the RS–Au–SR–Au–SR trimer sites, removing the central Au–SR–Au unit increases this further to $\eta = 0.30$. However, when the two outside SR ligands are removed from the trimer site, the hybridization of the highly disconnected central Au–SR–Au link increases to 0.63 and an Au(I)–thiolate structure is produced.

**The Role of Superexchange in Facilitating Long-Distance Interactions.** The previous analysis of the SR–Au–SR–Au–SR trimer indicates that not only do direct Au–Au bonds facilitate the broad *s*-orbital band of the gold adatoms but superexchange (70) through Au–S–Au bridges is also important [this applies for both Au *s*–*s* coupling (71) and *d*–*d* coupling (72)]. In our model, this superexchange effect is attributed as the cause of the broadening (Fig. 2) of the gold *s* bands when ligands are added to the $Au_{102}$ cluster to make $Au_{102}(RS)_{44}$. The significance of superexchange is that, when considering the gold–gold bonding topology, an Au–S–Au interaction should be considered as if it provides a direct Au–Au bond. Hence gold adatoms should be considered as having (at least) four connections to the surface,


enough to produce broad *s*-electron bands. To put this result in context, we note again that the electronic structure of even the gold dimer $Au_2$ is known for its similarity to bulk gold and its dissimilarity to that of typical molecules (62, 63).

**Emergence of a Simple Rule Describing Nanoparticle Growth.** The bonding changes revealed in Table 1 suggest that nanoparticles commence as small structures without great bulklike character; for these, the bonding occurs via reactive Au(I)–thiolate species. Nanoparticles grow so as to optimize the strong gold–gold *s*–*s* interactions, nobleizing the electronic structure. The nature of the gold–sulfur bonds adjusts accordingly, with Au(I)–thiolate character being minimized to form Au(0)–thiyl species. Evidence of significant Au(I)–thiolate character is therefore expected to be found only within nanoparticles much smaller than $Au_{102}(SR)_{44}$, and thorough analysis of DFT results for small systems should be highly revealing. Indeed, in the limit of very small clusters, the binding must reduce to the Au(I)–thiolate structures that are well established for small molecular species. Of interest in this regard too are scanning tunnelling microscopy (STM) break-junction experiments in which STM tips are run into SAMs and then withdrawn, pulling out monatomic gold wires that eventually break (73). This constitutes the reverse process to nanoparticle growth, taking stable Au(0)–thiyl interfaces and converting them to Au(I)–thiolates in solution.

Simple rules may be broken, however. If Au–S bonds are strong enough, then in aqueous solution addition of thiols to nanoparticles can dissolve the nanoparticle, converting Au(0) to Au(I) (74) to form identifiable thiolate species. Also, aromatic thiols in hexane can dissolve nanoparticles to form $Au(HSR)_2$ compounds without thiolate formation (75). These contrasting exceptions are easy to rationalize from the standpoint of initial Au(0)–thiyl monolayers and the balanced chemical forces that give rise to them.

**Binding Energies of Au Atoms to Surfaces and Nanoparticles.** Further insight into the SAM and nanoparticle assembly process can be gleaned by looking at the energies for the addition of single gold atoms to either Au(111) or to the $Au_{79}$ inner core of $Au_{102}(SR)_{44}$, energies also reported in Table 1. Adding adatoms in situ at their geometries in SAMs releases 2.0 eV energy on both Au(111) and nanoparticle dimer sites, reducing on nanoparticle trimer sites to 1.9 eV as a result of the increased *s*–*d* hybridization. This small variation is, however, indicative of the critical role played by the Au–Au bonds in controlling the properties of adatom-bound complexes. If such an atom is added in an optimized way to the nanoparticle core, the binding increases to 2.6 eV, the same value as that calculated for adding preformed RSAuSR units to the core (39). It is this feature that allows nanoparticles to form over a wide size range. Also of note is that the optimized Au–Au bond lengths in these SAMs vary over a large range, 3.1 ± 0.2 Å, indicating that these bonds are both strong and unusually flexible. Indeed, this flexibility is known to be associated with changes in *s*–*d* hybridization (23), but here it is shown to be integral to the ligand binding also. Substrate relaxation also significantly influences properties such as SAM surface-cell selection (18) and Au(111)–nanoparticle bonding differences (39).

**How Ag, Se, or Te Substitution Changes the Bonding.** Once the nature of Au–SR bonds are understood, the relative properties of related systems such as Au–SeR and Ag–SR bonds are easy to interpret. Au–Se bonds are both stronger and more structurally diverse than Au–S bonds (76). Contributions from covalent bonding depicted by structure **1b** decrease in going down the periodic table, whereas the dispersive contributions that dominate the binding pertinent to structure **2a** increase and so the observed increased bond strength is only interpretable by the Au(0)–thiyl description. This increased dispersive character to the bonding also explains the observed structural diversity. Conversely, Ag–SR bonding is known to be similar to that of Au–SR but the properties of the protecting ligands are distinctly more like thiolate species (77), as would be expected owing to the reduction of the dispersive contribution to the bonding and the associated increase in covalent character.

## A Conceptual Basis for Understanding the Chemical and Electrochemical Strategies for Making Either Protected Nanoparticles and Surfaces or Else Molecular Compounds and Thin Films

The nature of the Au–S bonding is critical to the understanding of the chemical and electrochemical reactions that make and destroy SAMs, nanoparticles, and thin films. The differences between the nonbonding description structure **2a** and the Au(I)–thiolate descriptions are not semantic as these descriptions depict different chemical species that may be independently produced. Chemical reactions proceed toward the species of lowest energy, but the initial conditions for the reaction may bring together species analogous to structure **2a** or species analogous to Au(I)–thiolates. Fig. 1 stresses this by showing the ground-state and excited-state singlet energy surfaces for bond dissociation, highlighting the asymptotic species that correspond to the various equilibrium structures. For example, Au(I) ions and thiolate anions may be prepared in solution and mixed together. A chemical reaction ensues that starts on the Au(I)–thiolate potential-energy surface. Conversely, adding electrons to a formed SAM results in reductive desorption, liberating thiolate anions as the asymptotic reaction product. The expected mechanisms and products of these reactions depend critically on whether or not the nonbonded form structure **2a** is considered to be the ground state rather than an Au(I)–thiolate.

First we consider electrochemical reaction paths for the destruction of SAMs by reductive desorption. This can easily be accounted for by the Au(0)–thiyl model, structure **2a**, as the adatom complex possesses a low-lying orbital that could accommodate an initial reactive thiolate intermediate that simply dissociates

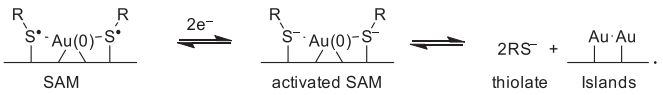


**[2]**

Most significantly, this process is seen to produce high-energy thiolate anions in solution. These are stable in polar aprotic solvents but in water undergo subsequent acid–base reactions depending on pH.

A significant aspect of the nonbonded form, structure **2a**, emphasized in Eq. **2** is that the sulfur atoms are represented as radicals. Naively, one would expect them therefore to undergo free-radical chemistry on the surface, making the gold surface catalytic for some chemical reaction. This is contrary to most observations; the SAM typically passivates the surface instead. The DFT calculations provide explanation for this anomaly. The sulfur orbital interacts significantly with the gold orbitals, delocalizing the radical character into the metal orbitals. At low surface coverage, this effect passivates the radical. At high coverage, the radical density becomes too high for this effect to operate, but the delocalization couples the sulfur atoms to each other via superexchange, just as superexchange through S couples Au atoms together, as discussed earlier. This effect is akin to those controlling ferromagnetic and antiferromagnetic couplings in materials and provides a weak bonding effect sufficient to spin pair the sulfur electrons, but this effect is not strong enough to warrant inclusion in energetics modeling. DFT reveals no significant change in energy when the wavefunctions are allowed to take on triplet character, indicating that the radicals are passivated and therefore free-radical chemistry on the surface is not expected.

Next we consider reaction paths for SAM production. SAMs are formed by exposing Au(111) to thiols or disulfides

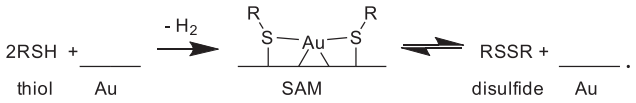


[3]

These processes are readily conceived as occurring along a radical pathway. Radicals such as Au(0) and S$^{\bullet}$ are unstable in solution and so cannot be brought together by long-range preassembly, but their involvement in the observed processes is understandable. However, whether or not Au(I)–thiolate species are present can be investigated by synthesizing the ions and bringing them together. Thiolate ions in alkaline media or in solvents that do not allow acid–base reactions are well-characterized stable chemical species. Au(I) ions (in their $d^{10}s^0$ ground state) can be made by, say, oxidizing gold electrodes. Both processes have been activated simultaneously using preparative electrochemistry in acetonitrile (78), using the anode and cathode reactions

$$\begin{aligned} \mathrm{Au(solid)} &\rightarrow \mathrm{Au^+(soln)} + e^- \\ \mathrm{RSH(soln)} + e^- &\rightarrow \mathrm{RS^-(soln)} + \frac{1}{2}\mathrm{H_2(gas)} \end{aligned} \quad . \qquad [4]$$

This allows $Au^+$ and $RS^-$ to meet and react in the solution. If SAMs are made of Au(I)–thiolates, then the SAM constituents have been preprepared, optimizing conditions for SAM production. Such a reaction is therefore envisaged as occurring under mild conditions and hence would be expected to be facilitated near the gold surface. Alternatively, if the SAMs are as depicted by structure **2a**, then when $Au^+$ and $RS^-$ ions meet they start on the high-energy excited-state Au(I)–thiolate potential energy surface, resulting in an exothermic reaction. Such a reaction would be expected to occur in solution and not need to be activated by the gold surface. Experimentally, what is observed is the solution reaction (78)

$$\mathrm{Au^+(soln)} + \mathrm{RS^-(soln)} \rightarrow \mathrm{AuSR(film)}, \qquad [5]$$

and the resulting Au(I)–thiolate film then precipitates onto the gold electrode. The experimental reaction conditions are optimized to etch gold surfaces to make thin films rather than to form protective SAMs, as expected if the SAM structure is **2a**; instead, the Au(I)–thiolate model of the SAM predicts that the reaction conditions were optimized for SAM production.

The known chemistry of gold nanoparticle formation leads to the same conclusions. Nanoparticles can be formed under very mild conditions such as via the reduction of Au(III) ions by citrate as in the classic Turkevich reaction (79–81) or even by thiols, e.g., by reactions in aqueous solution (82) of the form

$$\begin{aligned} (6m+2n)\mathrm{RSH} + 2m\mathrm{Au^{3+}} &\rightleftharpoons 2\mathrm{Au}_m(\mathrm{SR})_n \\ &+ 3m\mathrm{RSSR} + 6m\mathrm{H^+} + n\mathrm{H_2}, \end{aligned} \qquad [6]$$

in which the thiol reductant is sufficient to reduce Au(III) all of the way to Au(0) (82):

$$6\mathrm{RSH} + 2\mathrm{Au^{3+}} \rightleftharpoons 2\mathrm{Au^0} + 3\mathrm{RSSR} + 6\mathrm{H^+}. \qquad [7]$$

However, under different conditions such as those used in the Brust–Schiffrin synthesis (83), the reaction proceeds through the formation of Au(I)–thiolate intermediary compounds and films (84) and involve much stronger reducing agents. In the original synthesis (83), *p*-mercaptophenol was used as the thiol, and it was found that acetic acid was needed to be added to the reaction mixture to prevent reduction of the phenol by $NaBH_4$, a difficult process as the thiol must be reduced first (85) so the product is a dianion dissolved in a solvent of 5:1 methanol:water. If this phenol can be reduced then under similar conditions it is likely that aliphatic thiols could also be reduced, but in such reactions acid is rarely added to the mixture and so thiolate anions would be produced in solution. Au(I) species can be observed also in the reaction mixture, hence classic Brust–Schiffrin reactions would then result in the prepreparation of Au(I) and $RS^-$ species in solution. If these react during nanoparticle synthesis as they are known to do during electrochemical etching experiments in aprotic solvents (78), then Au(I)–thiolate molecular compounds or films would be expected to form. Indeed, such species are observable and can be isolated, characterized, and subsequently converted to nanoparticles (84) using conditions compatible with those used in direct syntheses.

## Identification of Thiolate Anions as Intermediates During Brust–Schiffrin Synthesis

Rationalization of known chemistry of gold surface reactions and nanoparticle formation reactions thus leads to the prediction that thiolate anions are intermediated during Brust–Schiffrin synthesis. This hypothesis is verified spectroscopically (*Supporting Information*), exposing hexanethiol to Brust–Schiffrin reaction conditions in the absence of the Au(III) reagent. Conversion of hexanethiol to hexanethiolate is observed by noting that the changes in the molecules' UV absorption spectrum match those produced by base hydrolysis, monitoring the disappearance of the SH Raman band. Therefore, the formation of thiolate anions can result not only from ionization of the SH group by alkaline media [the $pK_a$ of hexanethiol is 10.4 (86)] but also from the direct reaction of borohydride with the thiol group to yield $H_2$ and the thiolate anion, as is known also to occur with metal hydrides (see ref. 87 and references cited therein). The stability within the time scale of the nanoparticle synthesis in methanol is sufficiently long to allow this route for thiolate formation (88).

To date the Brust–Schiffrin synthesis has been applied over 4,000 times, yet detailed aspects of the mechanism remain unknown, and the situation is similar for alternate thiol-based nanoparticle synthesis methods such as those using aqueous solution. Understanding the nature of nanoparticle stabilization through structure **2a** has thus led to the discovery of an important intermediate species. This leads to an understanding of the conditions required for nanoparticle synthesis: if the reaction conditions are aprotic and are sufficiently reducing to enable thiolate anion production in solution, then nanoparticle formation proceeds via Au(I)–thiolate intermediary compounds that require further reduction before nanoparticles form; alternatively, if the reaction conditions inhibit thiolate formation, then the nanoparticles form directly through reactions with thiols.

## Nature of the Bonding Revealed Through Other Chemical Processes

Chemical substitution of the bridge-head carbon atom can also be used to differentiate between the possible valence states. Ligand exchange reactions on nanoparticles are known to proceed with thiol reactants and products (1). Many different mechanisms for this process have been found, including adsorption of the incoming species at defect sites followed by place exchange, as well as direct SN2-type ligand replacement (76, 89, 90). The SN2-type processes would be expected to involve a radical mechanism that includes hydrogen transfer between the incoming and outgoing thiol ligands and is the most obvious interpretation of the available data, whereas an Au(I)–thiolate description of the bonding would demand that proton loss and recapture occur independent of the SN2 reaction and is difficult to reconcile with the used experimental conditions (90). Moreover, that ligand exchange reactions can be performed at all indicates that the energetics of SAM and nanoparticle formation are only weakly dependent on the nature of nonchemically active ligands. This principle is in direct contrast to

that expected for Au(I)–thiolate structure **2c** as the latter depicts the bonding as arising from cancellation of large chemical forces driving ionic and covalent bonding, opposed by the Au $d^9s^1$ promotion energy. Hence even small effects on the binding caused by chemical substitution are expected to affect profoundly the net interaction, contrary to observation. Misinterpretation of very strong van der Waals forces as chemical bonds formed between high-energy states has been common for related systems such as benzene on Cu(110) as well (91).

## Conclusions

The usual classification scheme that labels AuSR-type molecules and materials as $d^{10}s^0$ Au(I)–thiolates is inappropriate to describe the bonding of sulfur compounds to gold surfaces and nanoparticles as it ignores the critical role of Au *s* to Au *s* interactions (supported by Au–S–Au superexchange) that passivates gold surface atoms and adatoms to give them noble character. This description also ignores the important effects of aurophilicity in determining the binding. Aurophilicity is the van der Waals force that provides a strong attraction between different gold atoms, which, by its nature, demands similar strong interactions between gold and other polarizable atoms such as sulfur.

Because gold surfaces and the surfaces of large nanoparticles are noble, chemisorption must be considered in terms of the interaction of the S *p* electron with a pair of Au *d* electrons, making the gold electronic configuration of an Au(I)–thiolate species $d^9s^1$. Species need to be characterized in terms of either this limiting form or else its alternate, nonbonded Au(0)–thiyl. All DFT calculations, supported by a wide range of spectroscopic, chemical, and electrochemical observations, indicate that the valence state of gold–sulfur interfaces is Au(0)–thiyl. The bond strength arises from a combination of the large van der Waals attraction energy akin to the aurophilic attraction, combined with perturbatively added chemisorption character arising from polarization effects and *s*–*d* hybridization effects.

The interpretations presented historically for DFT calculations and experimental results do not always conform to this description, however, and these reports need to be reinterpreted from this fully general perspective. In particular, the often-used description of gold–sulfur adatom complexes as "staples" (92)

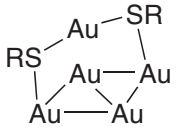


is misleading and should be discontinued; this description depicts the gold–sulfur bonding topology only and ignoring the critical gold–gold bonds. Even though these bonds are very malleable, they still contribute strongly to adatom-complex bonding, passivating the adatom *s* electrons to reduce the net gold–sulfur bonding strength. Superexchange interactions are critical not only because they lead to gold–gold interactions through intervening sulfur but also because they lead to sulfur–sulfur interactions through intervening gold.

For bonding in different configurations, a simple relationship is found linking the connectivity of particular atoms with the bulk to the amount of *s* character retained in the bonding and hence to the bond strength. A wide variety of phenomena are controlled by this effect including nanoparticle size control and STM break-junction measurements. The Au(0)–thiyl surface-bonding description allows for a consistent treatment of physisorption and chemisorption, linking smoothly to the properties of both established Au(I)–thiolate molecular compounds, of interfaces in which O, Se, Te, N, and C replace S, and of the aurophilic effect. Most significantly, it also explains how, when conditions are optimized to make Au(I)–thiolates, bare gold surfaces are etched while nanoparticles are not formed. It predicts the production of thiolate ion intermediated during Brust–Schiffrin synthesis, a feature then confirmed by experimental observation.

**ACKNOWLEDGMENTS.** We thank Prof. R. W. Berg for use of his specially built Raman spectrometer, and the Australian Research Council, the Danish Council for Independent Research, Technology and Production Sciences, the European Union FP7 Staff Exchange Program PIRSES-GA-2012-318990 – ELECTRONANOMAT, and National Computational Infrastructure for funding this research.

1. Sardar R, Funston AM, Mulvaney P, Murray RW (2009) Gold nanoparticles: Past, present, and future. *Langmuir* 25(24):13840–13851.
2. Hutchings GJ, Brust M, Schmidbaur H (2008) Gold—An introductory perspective. *Chem Soc Rev* 37(9):1759–1765.
3. Love JC, Estroff LA, Kriebel JK, Nuzzo RG, Whitesides GM (2005) Self-assembled monolayers of thiolates on metals as a form of nanotechnology. *Chem Rev* 105(4): 1103–1169.
4. Schmidbaur H (1995) Ludwig Mond Lecture. High-carat gold compounds. *Chem Soc Rev* 24:391–400.
5. Whitesides GM, Laibinis PE (1990) Wet chemical approaches to the characterization of organic surfaces: Self-assembled monolayers, wetting, and the physical-organic chemistry of the solid-liquid interface. *Langmuir* 6(1):87–96.
6. Maksymovych P, Voznyy O, Dougherty DB, Sorescu DC, Yates JT, Jr (2010) Gold adatom as a key structural component in self-assembled monolayers of organosulfur molecules on Au(1 1 1). *Prog Surf Sci* 85(5):206–240.
7. Häkkinen H (2012) The gold-sulfur interface at the nanoscale. *Nat Chem* 4(6):443–455.
8. Maksymovych P, Sorescu DC, Yates JT, Jr (2006) Gold-adatom-mediated bonding in self-assembled short-chain alkanethiolate species on the Au(111) surface. *Phys Rev Lett* 97(14):146103.
9. Mazzarello R, et al. (2007) Structure of a $CH_3S$ monolayer on Au(111) solved by the interplay between molecular dynamics calculations and diffraction measurements. *Phys Rev Lett* 98(1):016102.
10. Cossaro A, et al. (2008) X-ray diffraction and computation yield the structure of alkanethiols on gold(111). *Science* 321(5891):943–946.
11. Jadzinsky PD, Calero G, Ackerson CJ, Bushnell DA, Kornberg RD (2007) Structure of a thiol monolayer-protected gold nanoparticle at 1.1 A resolution. *Science* 318(5849): 430–433.
12. Sheppard DC, et al. (2011) Medium energy ion scattering investigation of methylthiolate-induced modification of the Au(111) surface. *Surf Sci* 605(1-2):138–145.
13. Maksymovych P, Sorescu DC, Voznyy O, Yates JT, Jr (2013) Hybridization of phenylthiolate- and methylthiolate-adatom species at low coverage on the Au(111) surface. *J Am Chem Soc* 135(13):4922–4925.
14. Yan J, et al. (2014) Controlling the stereochemistry and regularity of butanethiol self-assembled monolayers on au(111). *J Am Chem Soc* 136(49):17087–17094.
15. Ouyang R, et al. (2015) Intermixed adatom and surface-bound adsorbates in regular self-assembled monolayers of racemic 2-butanethiol on Au(111). *Chem Phys Chem* 16(5):928–932.
16. Nishigaki J, et al. (2012) A new binding motif of sterically demanding thiolates on a gold cluster. *J Am Chem Soc* 134(35):14295–14297.
17. Zhang J, Bilic A, Reimers JR, Hush NS, Ulstrup J (2005) Coexistence of multiple conformations in cysteamine monolayers on Au(111). *J Phys Chem B* 109(32): 15355–15367.
18. Wang Y, et al. (2011) Chain-branching control of the atomic structure of alkanethiol-based gold-sulfur interfaces. *J Am Chem Soc* 133(38):14856–14859.
19. Chaudhuri A, et al. (2009) The structure of the Au(111)/methylthiolate interface: New insights from near-edge x-ray absorption spectroscopy and x-ray standing waves. *J Chem Phys* 130(12):124708.
20. Solomon GC, et al. (2006) Understanding the inelastic electron tunnelling spectra of alkanedithiols on gold. *J Chem Phys* 124(9):094704.
21. Bacskay GB, Reimers JR, Nordholm S (1997) The mechanism of covalent bonding. *J Chem Educ* 74(12):1494.
22. Barton EJ, et al. (2014) ExoMol molecular line lists V: The ro-vibrational spectra of NaCl and KCl. *Mon Not R Astron Soc* 442(2):1821–1829.
23. Pyykkö P (2004) Theoretical chemistry of gold. *Angew Chem Int Ed Engl* 43(34): 4412–4456.
24. Tang Q, Jiang D-E (2014) Insights into the PhC≡C/Au Interface. *J Phys Chem C* 119(20): 10804–10810.
25. Zaba T, et al. (2014) Formation of highly ordered self-assembled monolayers of alkynes on Au(111) substrate. *J Am Chem Soc* 136(34):11918–11921.
26. Jansen M (2008) The chemistry of gold as an anion. *Chem Soc Rev* 37(9):1826–1835.
27. Bruening M, et al. (1997) Simultaneous control of surface potential and wetting of solids with chemisorbed multifunctional ligands. *J Am Chem Soc* 119(12):5720–5728.
28. Duwez A-S (2004) Exploiting electron spectroscopies to probe the structure and organization of self-assembled monolayers: A review. *J Elect Spectrosc Rel Phen* 134(2-3):97–138.
29. Bourg M-C, Badia A, Lennox RB (2000) Gold-sulfur bonding in 2D and 3D self-assembled monolayers: XPS characterization. *J Phys Chem B* 104(28):6562–6567.

30. Alloway DM, et al. (2003) Interface dipoles arising from self-assembled monolayers on gold: UV-photoemission studies of alkanethiols and partially fluorinated alkanethiols. *J Phys Chem B* 107(42):11690–11699.
31. De Renzi V, et al. (2005) Metal work-function changes induced by organic adsorbates: A combined experimental and theoretical study. *Phys Rev Lett* 95(4):046804.
32. Rodriguez JA, et al. (2003) Coverage effects and the nature of the metal-sulfur bond in S/Au(111): High-resolution photoemission and density-functional studies. *J Am Chem Soc* 125(1):276–285.
33. Howell S, et al. (2002) Molecular electrostatics of conjugated self-assembled monolayers on Au(111) using electrostatic force microscopy. *Langmuir* 18(13):5120–5125.
34. Méndez De Leo LP, de la Llave E, Scherlis D, Williams FJ (2013) Molecular and electronic structure of electroactive self-assembled monolayers. *J Chem Phys* 138(11): 114707.
35. Zhong C-J, Brush RC, Anderegg J, Porter MD (1998) Organosulfur monolayers at gold surfaces: Reexamination of the case for sulfide adsorption and implications to the formation of monolayers from thiols and disulfides. *Langmuir* 15(2):518–525.
36. Zhong C-J, Woods NT, Dawson GB, Porter MD (1999) Formation of thiol-based monolayers on gold: Implications from open circuit potential measurements. *Electrochem Commun* 1(1):17–21.
37. Konôpka M, Rousseau R, Stich I, Marx D (2004) Detaching thiolates from copper and gold clusters: Which bonds to break? *J Am Chem Soc* 126(38):12103–12111.
38. Bilić A, Reimers JR, Hush NS (2005) The structure, energetics, and nature of the chemical bonding of phenylthiol adsorbed on the Au(111) surface: Implications for density-functional calculations of molecular-electronic conduction. *J Chem Phys* 122(9):094708.
39. Reimers JR, Wang Y, Cankurtaran BO, Ford MJ (2010) Chemical analysis of the superatom model for sulfur-stabilized gold nanoparticles. *J Am Chem Soc* 132(24): 8378–8384.
40. Grönbeck H (2010) Thiolate induced reconstruction of Au(111) and Cu(111) investigated by density functional theory calculations. *J Phys Chem C* 114(38): 15973–15978.
41. Zhang T, Ma Z, Wang L, Xi J, Shuai Z (2014) Interface electronic structures of reversible double-docking self-assembled monolayers on an Au(111) surface. *Philos Trans A Math Phys Eng Sci* 372(2013):20130018.
42. Grönbeck H, Curioni A, Andreoni W (2000) Thiols and disulfides on the Au(111) surface: The headgroup-gold interaction. *J Am Chem Soc* 122(16):3839–3842.
43. Rusu PC, Brocks G (2006) Surface dipoles and work functions of alkylthiolates and fluorinated alkylthiolates on Au(111). *J Phys Chem B* 110(45):22628–22634.
44. de la Llave E, Clarenc R, Schiffrin DJ, Williams FJ (2014) Organization of alkane amines on a gold surface: Structure, surface dipole, and electron transfer. *J Phys Chem C* 118(1):468–475.
45. Frisch MJ, et al. (2009) *Gaussian 09, Revision D.01* (Gaussian, Inc., Pittsburgh, PA).
46. Brust M, Walker M, Bethell D, Schiffrin DJ, Whyman R (1994) Synthesis of thiol-derivatized gold nanoparticles in a two-phase liquid-liquid system. *J Chem Soc Chem Commun* 801–802.
47. Weisbecker CS, Merritt MV, Whitesides GM (1996) Molecular self-assembly of aliphatic thiols on gold colloids. *Langmuir* 12:3763–3772.
48. Nuzzo RG, Zegarski BR, Dubois LH (1987) Fundamental studies of the chemisorption of organosulfur compounds on Au(111) - Implications for molecular self-assembly on gold surfaces. *J Am Chem Soc* 109(3):733–740.
49. Yee CK, et al. (2003) Alkyl selenide- and alkyl thiolate-functionalized gold nanoparticles: Chain packing and bond nature. *Langmuir* 19(22):9450–9458.
50. Ansar SM, et al. (2011) Determination of the binding affinity, packing, and conformation of thiolate and thione ligands on gold nanoparticles. *J Phys Chem C* 115(3): 653–660.
51. Lustemberg PG, et al. (2008) Spontaneously formed sulfur adlayers on gold in electrolyte solutions: Adsorbed sulfur or gold sulfide? *J Phys Chem C* 112(30): 11394–11402.
52. Kurashige W, et al. (2014) Au25 clusters containing unoxidized tellurolates in the ligand shell. *J Phys Chem Lett* 5(12):2072–2076.
53. Wang L, He C, Zhang W, Li Z, Yang J (2014) Methanol-selective oxidation pathways on Au surfaces: A first-principles study. *J Phys Chem C* 118(31):17511–17520.
54. Gong J, Flaherty DW, Ojifinni RA, White JM, Mullins CB (2008) Surface chemistry of methanol on clean and atomic oxygen pre-covered Au(111). *J Phys Chem C* 112(14): 5501–5509.
55. Leff DV, Brandt L, Heath JR (1996) Synthesis and characterization of hydrophobic, organically-soluble gold nanocrystals functionalized with primary amines. *Langmuir* 12(20):4723–4730.
56. Cafe PF, et al. (2007) Chemisorbed and physisorbed structures for 1,10-phenanthroline and Dipyrido[3,2-a:2′,3′-c]phenazine on Au(111). *J Phys Chem C* 111(46): 17285–17296.
57. Schmidbaur H, Schier A (2008) A briefing on aurophilicity. *Chem Soc Rev* 37(9): 1931–1951.
58. Rangel T, et al. (2012) Band structure of gold from many-body perturbation theory. *Phys Rev B* 86(12-15):125125.
59. Han Y-K, Kim H, Jung J, Choi YC (2010) Understanding the magic nature of ligand-protected gold nanoparticle Au102(MBA)44. *J Phys Chem C* 114(17):7548–7552.
60. Li Y, Galli G, Gygi F (2008) Electronic structure of thiolate-covered gold nanoparticles: Au102(MBA)44. *ACS Nano* 2(9):1896–1902.
61. Gao Y, Shao N, Zeng XC (2008) Ab initio study of thiolate-protected Au102 nanocluster. *ACS Nano* 2(7):1497–1503.
62. McAdon MH, Goddard WA (1988) Charge density waves, spin density waves, and Peierls distortions in one-dimensional metals. I. Hartree–Fock studies of Cu, Ag, Au, Li, and Na. *J Chem Phys* 88:277–302.
63. McAdon MH, Goddard WA (1988) Charge density waves, spin density waves, and Peierls distortions in one-dimensional metals. 2. Generalized valence bond studies of copper, silver, gold, lithium and sodium. *J Phys Chem* 92(5):1352–1365.
64. Walter M, et al. (2008) A unified view of ligand-protected gold clusters as superatom complexes. *Proc Natl Acad Sci USA* 105(27):9157–9162.
65. Lavrich DJ, Wetterer SM, Bernasek SL, Scoles G (1998) Physisorption and chemisorption of alkanethiols and alkyl sulfides on Au(111). *J Phys Chem B* 102:3456–3465.
66. Wang Y, Hush NS, Reimers JR (2007) Formation of gold-methanethiyl self-assembled monolayers. *J Am Chem Soc* 129(47):14532–14533.
67. Hückel E (1931) Quantentheoretische beiträge zum benzolproblem. *Z Phys* 70(3-4): 204–286.
68. Vargas MC, Giannozzi P, Selloni A, Scoles G (2001) Coverage-dependent adsorption of CH3S and (CH3)S2 on Au(111): A density-functional study. *J Phys Chem B* 105(39): 9509–9513.
69. Hayashi T, Morikawa Y, Nozoye H (2001) Adsorption state of dimethyl disulfide on Au(111): Evidence for adsorption as thiolate at the bridge site. *J Chem Phys* 114(17): 7615–7621.
70. McConnell HM (1961) Intramolecular charge transfer in aromatic free radicals. *J Chem Phys* 35:508–515.
71. Reimers JR, Hush NS (1990) Electron and energy transfer through bridged systems. II. Tight binding linkages with zero asymmetric band gap. *Chem Phys* 146(1-2):89–103.
72. Reimers JR, Hush NS (1994) Electron and energy transfer through bridged systems. III. Tight binding linkages with finite asymmetric band gap. *J Photochem Photobiol Chem* 82(1-3):31–46.
73. Muller KH (2006) Effect of the atomic configuration of gold electrodes on the electrical conduction of alkanedithiol molecules. *Phys Rev B* 73(4):045403.
74. Shichibu Y, et al. (2007) Extremely high stability of glutathionate-protected $Au_{25}$ clusters against core etching. *Small* 3(5):835–839.
75. Wang F, He C, Han M-Y, Wu JH, Xu GQ (2012) Chemical controlled reversible gold nanoparticles dissolution and reconstruction at room-temperature. *Chem Commun (Camb)* 48(49):6136–6138.
76. Hohman JN, et al. (2014) Exchange reactions between alkanethiolates and alkaneselenols on Au111. *J Am Chem Soc* 136(22):8110–8121.
77. Perera GS, et al. (2014) Ligand desorption and desulfurization on silver nanoparticles using sodium borohydride in water. *J Phys Chem C* 118(19):10509–10518.
78. Chadha RK, Kumar R, Tuck DG (1987) The direct electrochemical synthesis of thiolato complexes of copper, silver, and gold; The molecular structure of $[Cu(SC_6H_4CH_3\text{-}o)(1,10\text{-phenanthroline})]_2.CH_3CN$. *Can J Chem* 65(6):1336–1342.
79. Ji X, et al. (2007) Size control of gold nanocrystals in citrate reduction: The third role of citrate. *J Am Chem Soc* 129(45):13939–13948.
80. Kimling J, et al. (2006) Turkevich method for gold nanoparticle synthesis revisited. *J Phys Chem B* 110(32):15700–15707.
81. Turkevich J, Stevenson PC, Hillier J (1951) A study of the nucleation and growth processes in the synthesis of colloidal gold. *Discuss Faraday Soc* 11:55–75.
82. Negishi Y, Tsukuda T (2003) One-pot preparation of subnanometer-sized gold clusters via reduction and stabilization by meso-2,3-dimercaptosuccinic acid. *J Am Chem Soc* 125(14):4046–4047.
83. Brust M, Fink J, Bethell D, Schiffrin DJ, Kiely C (1995) Synthesis and reactions of functionalized gold nanoparticles. *J Chem Soc Chem Commun* 16:1655–1656.
84. Corbierre MK, Lennox RB (2005) Preparation of thiol-capped gold nanoparticles by chemical reduction of soluble Au(I)–thiolates. *Chem Mater* 17(23):5691–5696.
85. Armstrong D, Sun Q, Schuler RH (1996) Reduction potentials and kinetics of electron transfer reactions of phenylthiyl redicals: Comparisons with phenoxyl radicals. *J Phys Chem* 100(23):9892–9899.
86. Almand G, Gorin G (1961) Ionization constant of hexanethiol from solubility measurements. *J Org Chem* 26:4682–4684.
87. Smith MB, Wolinsky J (1998) Reaction of thiols with $LiAlD_4$, a mechanistic study. *J Chem Soc, Perkin Trans 2*:1431–1434.
88. Lo C-tF, Karan K, Davis BR (2007) Kinetic studies of reaction between sodium borohydride and methanol, water. *Ind Eng Chem Res* 46(17):5478–5484.
89. Kassam A, Bremner G, Clark B, Ulibarri G, Lennox RB (2006) Place exchange reactions of alkyl thiols on gold nanoparticles. *J Am Chem Soc* 128(11):3476–3477.
90. Ni TW, Tofanelli MA, Phillips BD, Ackerson CJ (2014) Structural basis for ligand exchange on Au(25)(SR)(18). *Inorg Chem* 53(13):6500–6502.
91. Bilić A, Reimers JR, Hush NS, Hoft RC, Ford MJ (2006) Adsorption of benzene on copper, silver, and gold surfaces. *J Chem Theory Comput* 2(4):1093–1105.
92. Jiang D-E, Tiago ML, Luo W, Dai S (2008) The "staple" motif: A key to stability of thiolate-protected gold nanoclusters. *J Am Chem Soc* 130(9):2777–2779.
93. Frisch MJ, et al. (2009) *Gaussian 09, Revision C.09* (Gaussian, Inc., Pittsburgh, PA).
94. Yanai T, Tew DP, Handy NC (2004) A new hybrid exchange-correlation functional using the Coulomb-attenuating method (CAM-B3LYP). *Chem Phys Lett* 393(1-3): 51–57.